Quantitative Phase Imaging of Cells in Flow

Silvia Ceballos, Han Sang Park, Will J. Eldridge and Adam Wax

Department of Biomedical Engineering, Duke University, Durham, NC

http://bios.bme.duke.edu

DUKE UNIVERSITY
Fitzpatrick Institute for Photonics

Introduction and motivation

To advance quantitative phase imaging (QPI) as a diagnostic tool, it is necessary to develop it into a high throughput system. Our method is to use an off-axis Mach-Zehnder interferometer to image red blood cells (RBCs) flowing through a micro-chamber with a height of 8.60 µm.

To accurately acquire phase images of flowing cells, it is necessary to find a precise focal plane of the sample. To do so, we implemented four different algorithms that have been proven to work well for static cells on microscope slides. We use optical volume (OV) as a benchmark for quantitative comparisons of the different algorithms and the effects of defocus.

To effectively use this method, the QPI system would need to image the sample at different orientations to find the minimum range of OV across orientations, or use microchannels with proper dimensions to prevent the cells from tumbling, which in any case, influences the throughput of the system. In summary, we have developed a new approach to accurately obtain phase images of cells during flowing, overcoming the challenge of digital refocusing for these kind of setups.

Methods

Quantitative phase imaging

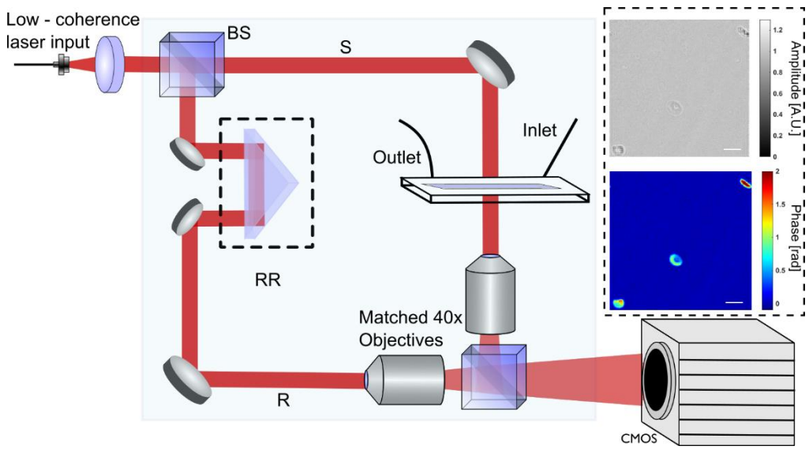

Fig 1. QPI system diagram. Path-matched sample (S) and reference (R) beams create off-axis interferograms imaged by a CMOS camera, (BS) beam splitter, (RR) retroreflectors. Inset: Amplitude and phase images of red blood cells flowing through the chamber. Scale bar = 5 µm.

Development of flow chambers

Chambers were fabricated using SU-8 photoresists. Coverslips (VWR #1.5, 22x40mm) were spin coated with SU8 (Microchem) in a headway spin coater. Then, the substrates were exposed to a pattern mask using a UV lamp on a Karl Suss MA6 mask aligner. After the development process, the height of the photoresists was measured to be 8.60 µm using a profilometer with 5x5mm of open space. Then, the developed chamber was bonded to a glass slide with both inlet and outlet using a customized manual press leveraging bolted joint design [1] to apply controlled pressure using a torque wrench.

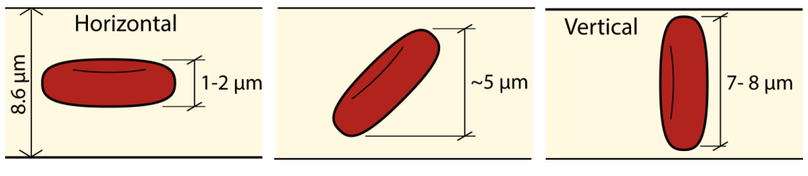

Fig 2. Schematic of the cells flowing through the chamber. Different RBC positions and orientations as it tumbles through the chamber.

Watch the video here:

Results

Digital refocusing and Optical Volume

$$\mathrm{OV}(t) = \iint_{x,y} \Delta OPL(x,y,t)\,dxdy$$

$$= \iint_{x,y} \Delta n(x,y,t) \cdot h(x,y,t)\,dxdy = \iint_{x,y} \Delta\phi(x,y,t)\frac{\lambda}{2\pi}\,dxdy$$

Where ΔOPL refers to the changes in optical path length, $h(x,y,t)$ is the height map of the object, $\Delta n(x,y,t)$ is the refractive index map and $\Delta\phi(x,y,t)$ is the phase map.

Refocusing vs optical volume

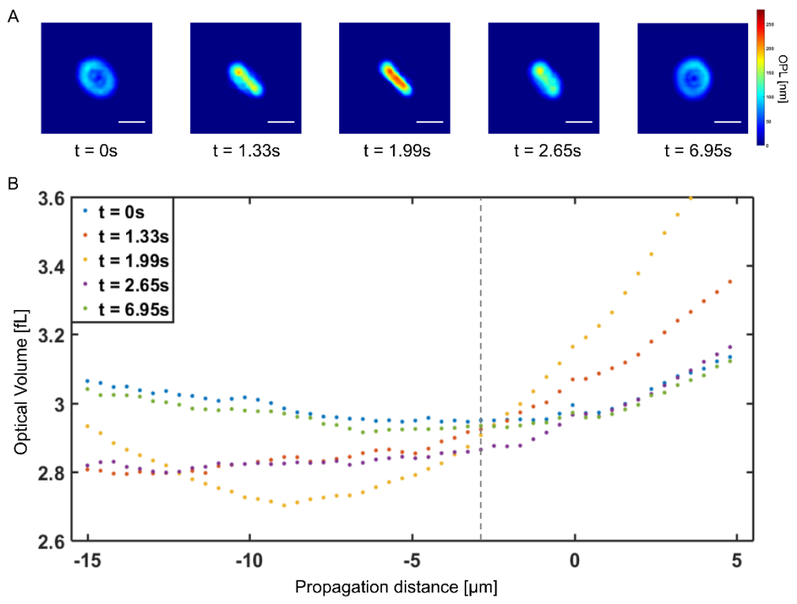

Fig 3. Influence of defocus. (A) Images of tumbling RBCs at different orientations. Scale bar = 5 µm (B) Optical volume of RBCs in (A) calculated at different propagation distances. Dashed line: Minimum range of OV = -3.28 µm.

Parameters for refocusing

For a N_x by N_y image, $g(x,y)$, the following metrics were calculated [2]:

$$\textbf{Variance} = \frac{1}{N_x N_y}\sum_{x,y}[g(x,y)-\bar{g}]^2$$

$$\textbf{Gradient} = \sum_{x=1}^{N_x-1}\sum_{y=1}^{N_y-1}\sqrt{[g(x,y)-g(x-1,y)]^2+[g(x,y)-g(x,y-1)]^2}$$

Tamura Coefficient and Gini Index algorithms are based on edge sparsity using the gradient of the complex optical wavefront [3, 4]:

$$\textbf{Tamura Coefficient}(\mathbf{c}) = \sqrt{\sigma(\boldsymbol{c})/\langle \boldsymbol{c}\rangle}$$

where $\boldsymbol{c}$ is the data vector (gradient of complex field) of size N and σ is the standard deviation.

$$\textbf{Gini Index}(\mathbf{c}) = \frac{2}{N}\sum_{k=1}^{N}\frac{k}{N}\tilde{a}_{[k]} - 1 - \frac{1}{N}$$

Where $a_{[k]}$ $(k = 1,\dots,N)$ are the sorted entries of $\mathbf{c}$ in ascending order, and $\tilde{a}_{[k]} = \frac{a_{[k]}}{\langle \mathbf{c}\rangle}$ are the sorted entries normalized by the mean $\langle \mathbf{c}\rangle$.

RangeOV: The propagation distance at which the range of OVs of different orientations of the cell is minimum [5].

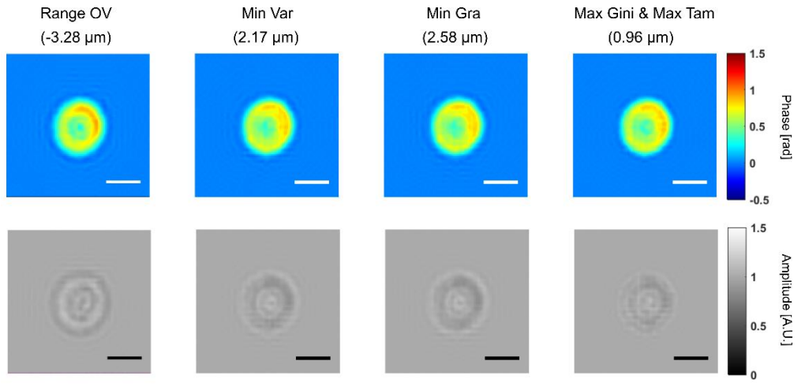

Fig 4. Phase and amplitude images of RBC. Phase maps of a RBC at refocus distance calculated using minimum range of OV, Min Var, Min Gra, Max Gini and Max Tamura at the top and corresponding amplitude maps at the bottom. Scale bar = 5µm.

Accurate refocusing using optical volume

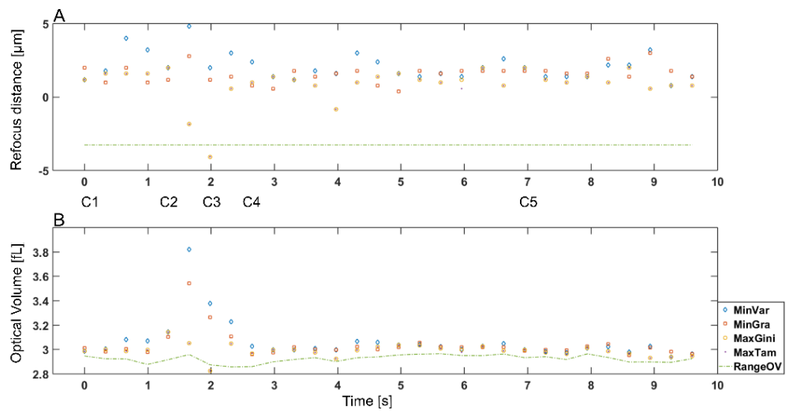

Fig 5. OV of tumbling cell refocused using different parameters. (A) Focusing distance for a tumbling cell calculated using different parameters: Min Var, Min Gra, Max Gini and Max Tamura (B) Optical volume of the tumbling RBC propagated by focusing distances calculated using different metrics shown in (A). C1 – C5 correspond to the five time points shown in Fig 3A throughout the flow.

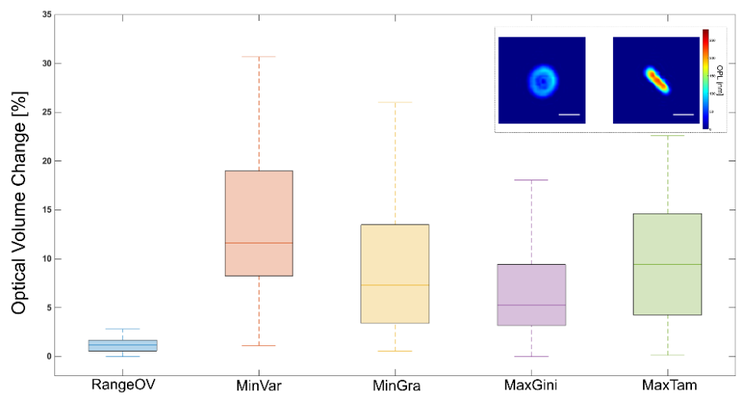

Fig 6. Optical volume change using different metrics. Optical volume changes between horizontal and vertical RBCs during flow using focusing distances determined by Min Var, Min Gra, Max Gini, Max Tamura and minimum range of OV (N=50) are 1.39 ±1.09%, 15.21 ±11.42%, 9.31 ±7.61%, 7.48 ±7.25%, and 9.94 ±6.02%, respectively. Inset: Example images of horizontal and vertical RBCs respectively. Scale bar = 5 µm.

RBCs show orientation-dependent absorption

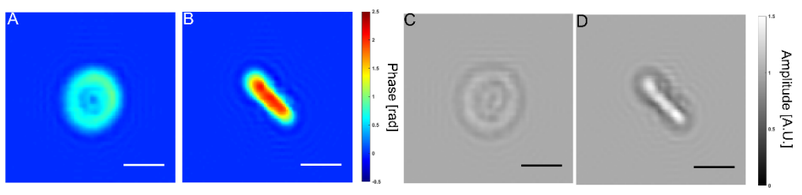

Fig 7. Phase and amplitude images of horizontal and vertical RBCs. (A) Phase map of a horizontal RBC (B) Phase map of a vertical RBC (C) Amplitude map of horizontal RBC (D) Amplitude map of vertical RBC. Scale bar = 5 µm.

Acknowledgements

Grant support from NSF (CBET 1604562), NIH (1R21-ES029791) and financial funding from Duke University are gratefully acknowledged. We also thank members of the BIOS lab for helpful discussions.

References

[1] S. Serra, A. Schneider, K. Malecki, S. Huq, and W. Brenner, "A simple bonding process of SU-8 to glass to seal a microfluidic device," in *Proceedings of 3rd International Conference on Multi-Material Micro Manufacture, Borovets, Bulgaria*, 2007, pp. 3-5.

[2] P. Langehanenberg, B. Kemper, D. Dirksen, and G. von Bally, "Autofocusing in digital holographic phase contrast microscopy on pure phase objects for live cell imaging," *Appl Opt,* vol. 47, no. 19, pp. D176-82, Jul 1 2008.

[3] M. Tamamitsu, Y. Zhang, H. Wang, Y. Wu, and A. Ozcan, "Comparison of Gini index and Tamura coefficient for holographic autofocusing based on the edge sparsity of the complex optical wavefront," *arXiv,* vol. 1708.08055, pp. 1-9, 2017.

[4] Y. Zhang, H. Wang, Y. Wu, M. Tamamitsu, and A. Ozcan, "Edge sparsity criterion for robust holographic autofocusing," *Opt Lett,* vol. 42, no. 19, pp. 3824-3827, Oct 1 2017.

[5] M. T. Rinehart, H. S. Park, and A. Wax, "Influence of defocus on quantitative analysis of microscopic objects and individual cells with digital holography," *Biomedical optics express,* vol. 6, no. 6, pp. 2067-2075, 2015.